HIGH ENERGY TEST OF CONDUCTIVE PLASTIC PROPORTIONAL TUBE ELECTROMAGNETIC CALORIMETER WITH CONICAL TOWER GEOMETRY

Y.Hayashide, T.Kamon, S.Kim, K.Kondo, S.Miyashita,
H.Miyata, F.Sato, Y.Takaiwa, A.Yamashita
University of Tsukuba, Ibaraki-ken, Japan,
S.Mikamo, M.Mishina
National Laboratory for High Energy Physics, KEK, Ibaraki-ken, Japan,
Y.Muraki
Institute for Cosmic Ray Research, University of Tokyo,
Tanashi-shi, Tokyo, Japan,
A.Murakami
Saga University, Saga-shi, Japan,
M.Atac, J.E.Freeman, D.R.Hanssen, J.C.Urish, R.Yamada, J.Yoh
Fermi National Accelerator Laboratory, Batavia, IL 60510, U.S.A.

SUMMARY

A prototype electromagnetic calorimeter module has been constructed using conductive plastic proportional tubes stacked with lead panels. Complete conical towers were formed by finely segmented pick-up electrodes etched on copper clad G-10 panels between which tube arrays were sandwitched.

The module was tested by high energy electron and hadron beams up to 175 GeV. Excellent energy and position resolutions were obtained. Rejection of pions against electrons was studied.

1. INTRODUCTION

In a continuing effort of prototyping the end cap electromagnetic calorimeter for the Fermilab Collider Detector Facility[1], we have built a 30 sector of the cylindrical calorimeter system in full size in radius as sketched in Fig. 1. Based on quite successful experience with the previous prototype module[2] we employed basically the same structure of the proportional tube layers in which a conductive plastic tube array was sandwitched with G-10 panels. The copper clad on G-10 was etched into pick-up electrodes which were flared with depth of the layer to form conical towers projected from the center of the interaction region.

In the following we discuss the structure of the module, beam test arrangement, and test results by electron and hadron beams up to 175 GeV. We summarize the results in the last chapter.

2. STRUCTURE OF THE PROTOTYPE MODULE

The basic structure was almost the same as the previous prototype module. An array of extruded conductive plastic tubes of 7 mm high x 10 mm wide cells, as shown in Fig. 2, was sandwitched between two 30° sector G-10 panels as shown in Fig. 3. 50 μm gold plated tungsten wire was used as the anode wires. The radial dimension of the G-10 panels and the pad and the strip patterns, shown in Figs. 4a, b, and c, closely simulated the final system. Thirtyeight such chamber layers were then interleaved with 3 mm calcium loaded lead panels. The pads were etched on G-10 panel on one side of every chamber layer and the θ- and the φ-strips were etched on the G-10 panels on the opposite side of the sixth through the twenty fifth chamber layer. The θ- andthe φ-strip layers were interleaved with each other. Otherwise the opposite sides of the chamber layers were plane copper surface grounded electrically. All the pads and strips were connected to edge card connectors at the outer circumferences of the G-10 panels by strip lines. The pad and strip patterns were flared with the depth to form conical towers of each well defined solid angle with respect to the center of the interaction region which was assumed to be on the center axis of the sector 188 cm distant

from the surface of the module. The pads at the same polar and azimuthal angles are connected together in depth, directly by flat cables, into three longitudinal segments. θ- and φ- strips are connected together into two longitudinal segments. The configuration is listed in Table 1.

All the anode wires in the sasme chamber layer were connected together through individual 100 ohm resistors in series and connected to a high voltage bus line through a 100 kohm resistor. The same point was branched to a read-out signal cable through a blocking capacitor.

3. BEAM TEST ARRANGEMENT

The beam test was done at the Fermilab M-4 line. A pure electron beam with energy up to 175 GeV was produced by converting a neutral beam by a lead block after the charged particles were swept away. Without any other electron identification, the hadron contamination was estimated to be less than 10^{-3} judging from the on-line pulse height distribution in Figs. 5a, b, and c. Particle momenta were measured with an r.m.s. error of 0.14 % event-by-event by a string of magnets and 1 mm-spacing pwc sets before and after the magnets. The beam profile was defined as 3 cm x 3 cm by three trigger counters and a large veto counter with a hole at the middle.

The calorimeter module was placed on a mount rotatable horizontally around a pivot point that simulated the center of the interaction region, and vertically around the simulated beam axis. Thus the beam could be injected straight into any selected pad tower.

All of the signals were fed directly into LRS 2285A 15 bit ADC modules by 280 nsec long RG58C/U cables. Since the signals from the pads and strips were of positive polarity, they were inverted by small ferrite core transformers. 1 to 4 μsec wide gate was used.

The gas was a 50 %-50 % argon-ethane mixture fed through an ethylalcohol bubbler kept at 0°C.

4. BEAM TEST RESULTS

The first part of the test was devoted to studying the general response of the calorimeter. Figs. 6a and b show typical signal shapes from pad towers and anode wires. The rise times of about 60 nsec observed in these photographs are in good agreement with the average transit time to the anode wire of the secondary electrons created uniformly in each of the tube cells by the shower. Since the particle rate at the real experiment is not expected to be high, the tail of the pad signal is not problematic.

Fig. 7 is an on-line display of the scatter plot of anode wire signal vs. pad signal for 25, 50, and 75 GeV electrons showing good correlations between them.

In order to determine the operating high voltage, several quantities were measured while varying the high voltage from 1.7 kV to 2.1 kV. A logarithmic plot of the gain was linear against the high voltage at lower voltage and showed breaks at 2 and 1.95 kV for 50 GeV and 100 GeV electrons, respectively, with a gain of 3 pC/GeV for 2 kV. The gain change was a factor of 2.4 per 100 V. These breaks corresponded to the deviation of the linear relationship of the gain versus the electron energies. These saturation points depended on the gas gain which was observed to be very sensitive to the gas purity. With the gas gain of 3 pC/GeV the gain was linear up to 125 GeV and showed mild saturation up to 1.2 % at 150 GeV.

With various gas gains, energy resolution was plotted against the

high voltage. In all cases there were optimum points around 2 kV which corresponded to the starting point of the saturation. This is consistent with the idea of suppression of the Landau tail without saturating the main minimum ionizing peak.[3]

A typical energy resolution plotted against $1/\sqrt{E}$ is shown in Fig.8. It is seen that the energy resolution is essentially the same for the pad signal and wire signal. Taking account of the unit sampling thickness t of 0.563 rad. l., the energy resolution is equivalent to 29 % $\sqrt{t/E}$.

Using the lateral distribution of the shower within neighboring towers, the shower centroid was calculated event-by-event and compared with the hit point measured by the preceding beam pwc's. The r.m.s. deviation thus calculated, as illustrated in Fig.9, was 1 mm or better at 50 GeV and above. Such a resolution will be quite useful in rejecting neutral background in the colliding beam experiment.

One of the major objectives of the present test was to confirm uniformity of the pad response independent of the sizes and their capacitances. Fig. 10 shows the ratio of the summed pad signals to the summed wire signals over various positions along the radius. Disregarding the fall off at both ends where the signal leaks out, the ratio is uniform to $\pm$ 3 % or less. The above mentioned position resolution was also observed to be well uniform over the same range.

Pion discrimination was studied using a mixed negative charged particle beam. Since it is expected that momentum measurement by tracking chamber is deteriorated at smaller angles in the real experimental situation of the Collider Detector Facility, we tried to discriminate against pions of the energies up to four times higher than the electrons to be detected. The algorithms studied were to cut the events which fell outside the region of electrons in the following distributions; total energy, energy deposit in the first pad segment, energy deposit in the third pad segment, and the lateral shower profile at the second pad segment. Figs. 11 a and b show typical trends of pion rejection against the retained electron efficiencies. It is seen that in the present energy region where pion charge exchange cross section is small, the comparison of the tail of the electromagnetic shower with the still developing hadronic shower is a powerful tool for pion rejection. It was found that almost independent of the incident energy, the pion rejection factor was 5×10^{-3} or better.

5. CONCLUSION

It was again demonstrated that conductive plastic tubes with outside pick-up electrodes were adequate as the proportional tube element which satisfied our requirement of ruggedness and also ease of making conical tower geometry.

It was observed that the energy resolution was optimized at the end of the proportional region. At the optimum voltage, 2 kV, an energy resolution of 29% $\sqrt{t/E}$ was obtained.

The rise time of the pad signals with many pads connected together was identical with the wire signals.

The shower centroid calculated from the measured sharing of the shower energy between the adjacent pad towers was found to give the true hit point with an accuracy of 1 mm or better at and above 50 GeV.

The response of the pads was uniform within $\pm$ 3 % over wide range of the radial positions.

Within the present energy region a pion rejection of better than 5 x

ACKNOWLEDGEMENT

The authors wish to express their sincere gratitude to M.Hrycyk, W.Coleman, J.Layman and, W.Ewer for their skillful work in the preparation, and to W.Baker, D.Green, R.Schailey and other Meson Lab staff for their fine support and modifying the M-4 line for the test.

REFERENCES

1) DESIGN REPORT FOR THE FERMILAB COLLIDER DETECTOR FACILITY, August 1981.
2) M.Atac, et al, IEEE Trans. NS-29 (1982) 368.
3) M.Atac, et al, Fermilab FN-368(1982). To be published in Nucl. Instr. Meth..

TABLE 1

FIGURE CAPTIONS

Fig. 1 : Sketch of the prototype 30 sector of the cylindrical end cap electromagnetic calorimeter. The outer radius is about 140 cm which is close to the final system.

Fig. 2 : Cross sectional dimensions of conductive plastic tubes.

Fig. 3 : Configuration of a unit layer. The sketch of the G-10 panel between the lead panel and the tube array is only to show the pattern of the signal strip lines on the back of the pad-etched G-10 panels. The G-10 panels on this side have either θ- or φ-strips or an un-etched ground plane. Also the tube orientation is different from the real configuration to show the tube cross sections.

Fig. 4 : Cathode pick-up electrode patterns;
a: Pads, b: θ-strips, c: φ-strips.

Fig. 5 : On-line pulse height distributions of summed anode wire signals at 1.8 kV for electrons;
a: 50 GeV, b: 100 GeV, c: 175 GeV.

Fig. 6 : Pulse shape of the signals from the second segment of a pad tower at η = 1.475 (θ = 25.8°) and the wire signal from the twelfth layer. The signals were brought to an oscilloscope via 280 nsec long RG58C/U and terminated with 50 ohms. H.V. = 1.9 kV, vert. scale = 5 mV/div.
a: Horiz. scale = 50 nsec/div,
b: Horiz. scale = 500 nsec/div.

Fig. 7 : Scatter plot of the summed pad signals vs. summed wire signals for 25, 50, and 75 GeV electrons at 1.95 kV.

Fig. 8 : The energy resolution at the optimum voltage.

Fig. 9 : R.m.s. deviation of the shower centroid in the direction of the radius from the hit point measured by the beam pwc's. η = 1.475 (θ = 25.8°).

Fig.10 : Uniformity of the pad to wire signal ratio along the radius.

Fig.11 : Pion rejection for various cuts;
a: 100 GeV pions against 50 GeV electrons,
b: 100 GeV pions against 100 GeV electrons.

TABLE 1
Conductive plastic proportional tube electromagnetic calorimeter configuration.

All 38 chambers have pad patterns on one side. Chambers No. 6 through No. 25 have strips on the other side, θ-strips on even-numbered chambers and φ-strips on odd-numbered chambers.

Vessel Wall Fe 1/2 in. 0.722 rad l.
Holder Plate Al 1 in. 0.285 rad l.

Chamber No.				
1	Pad Segment-I 2.82 rad l.			
2				
3				
4				
5				
6		θ-strip No. 1	θ-strip Segment-I	φ-strip No. 1
7				φ-strip Segment-I
8		θ-strip No. 2		φ-strip No. 2
9				
10		θ-strip No. 3		φ-strip No. 3
11				
12	Pad Segment-II 11.26 rad l.	θ-strip No. 4		φ-strip No. 4
13				
14		θ-strip No. 5		φ-strip No. 5
15				
16		θ-strip No. 6	θ-strip Segment-II	φ-strip No. 6
17				φ-strip Segment-II
18		θ-strip No. 7		φ-strip No. 7
19				
20		θ-strip No. 8		φ-strip No. 8
21				
22		θ-strip No. 9		φ-strip No. 9
23				
24		θ-strip No.10		φ-strip No.10
25				
26	Pad Segment-III 7.32 rad l.			
27				
28				
29				
30				
31				
32				
33				
34				
35				
36				
37				
38				

TOTAL 22.40 rad l.

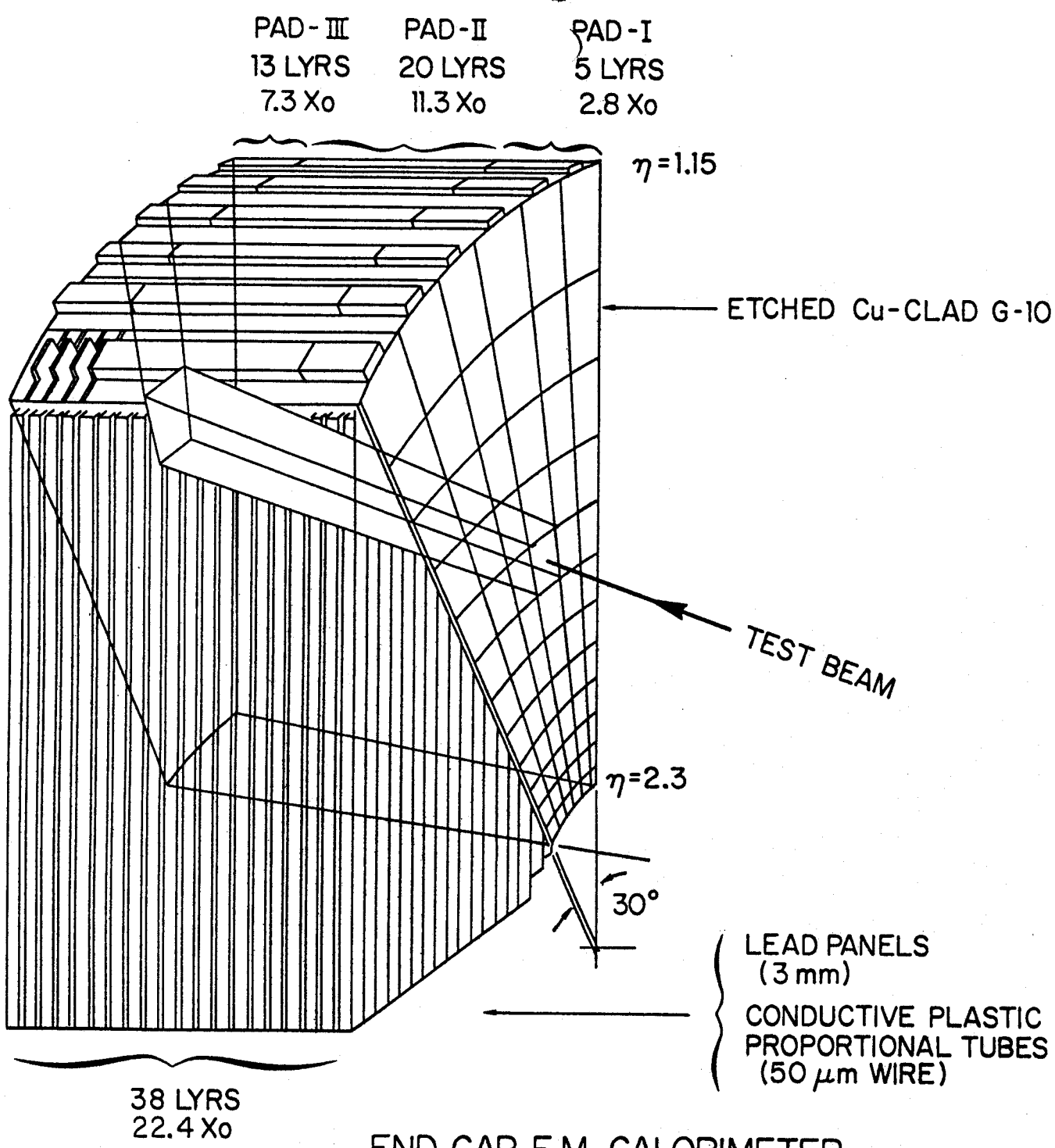

END CAP E.M. CALORIMETER
PROTOTYPE MODULE

FIG. 1

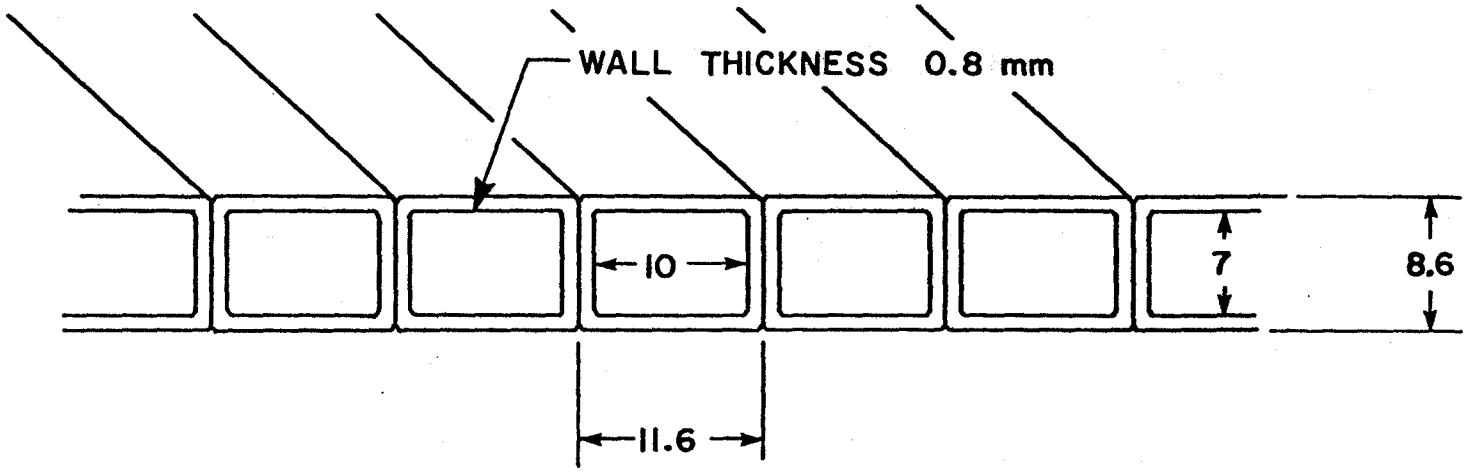

FIG. 2

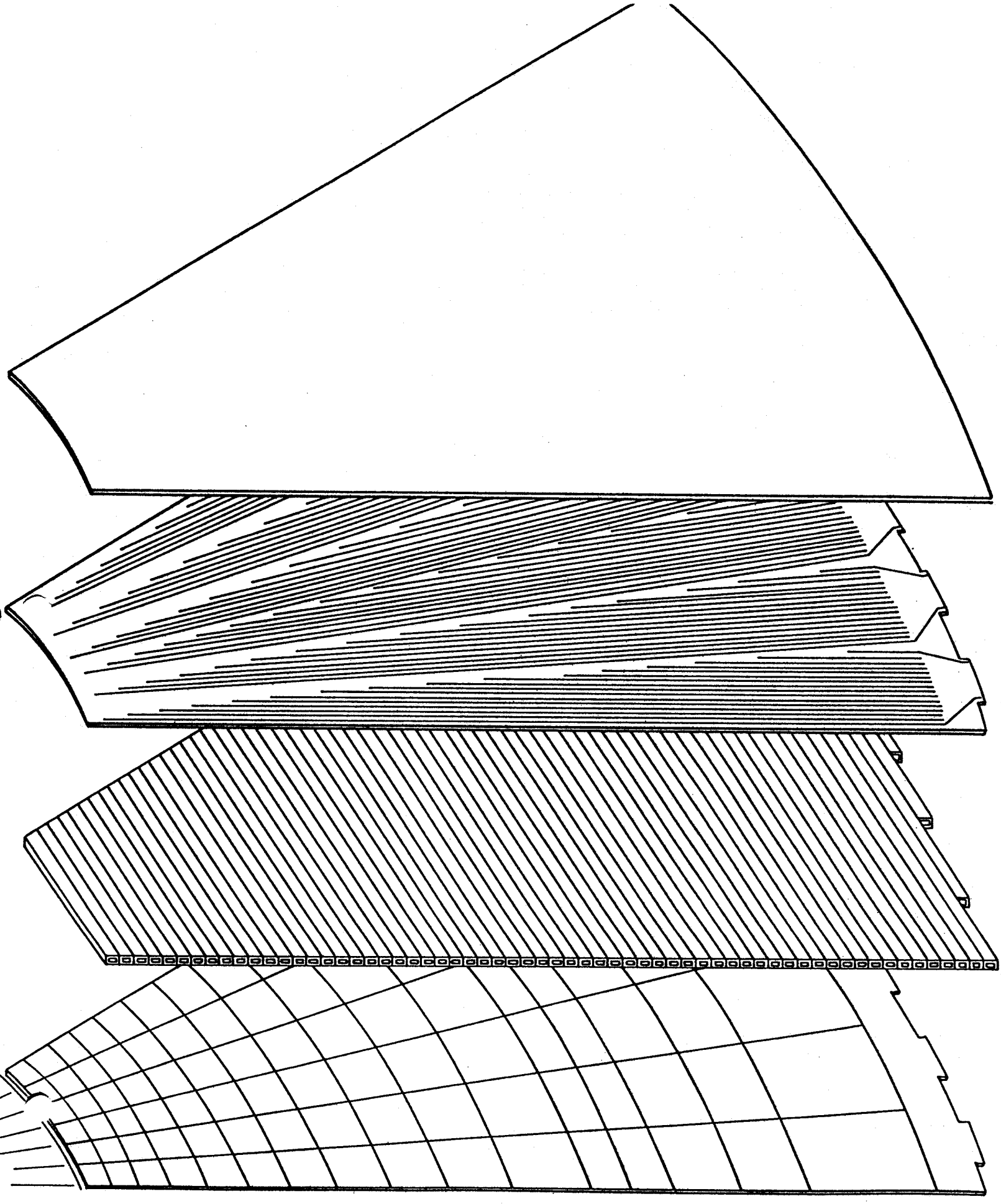

FIG. 3

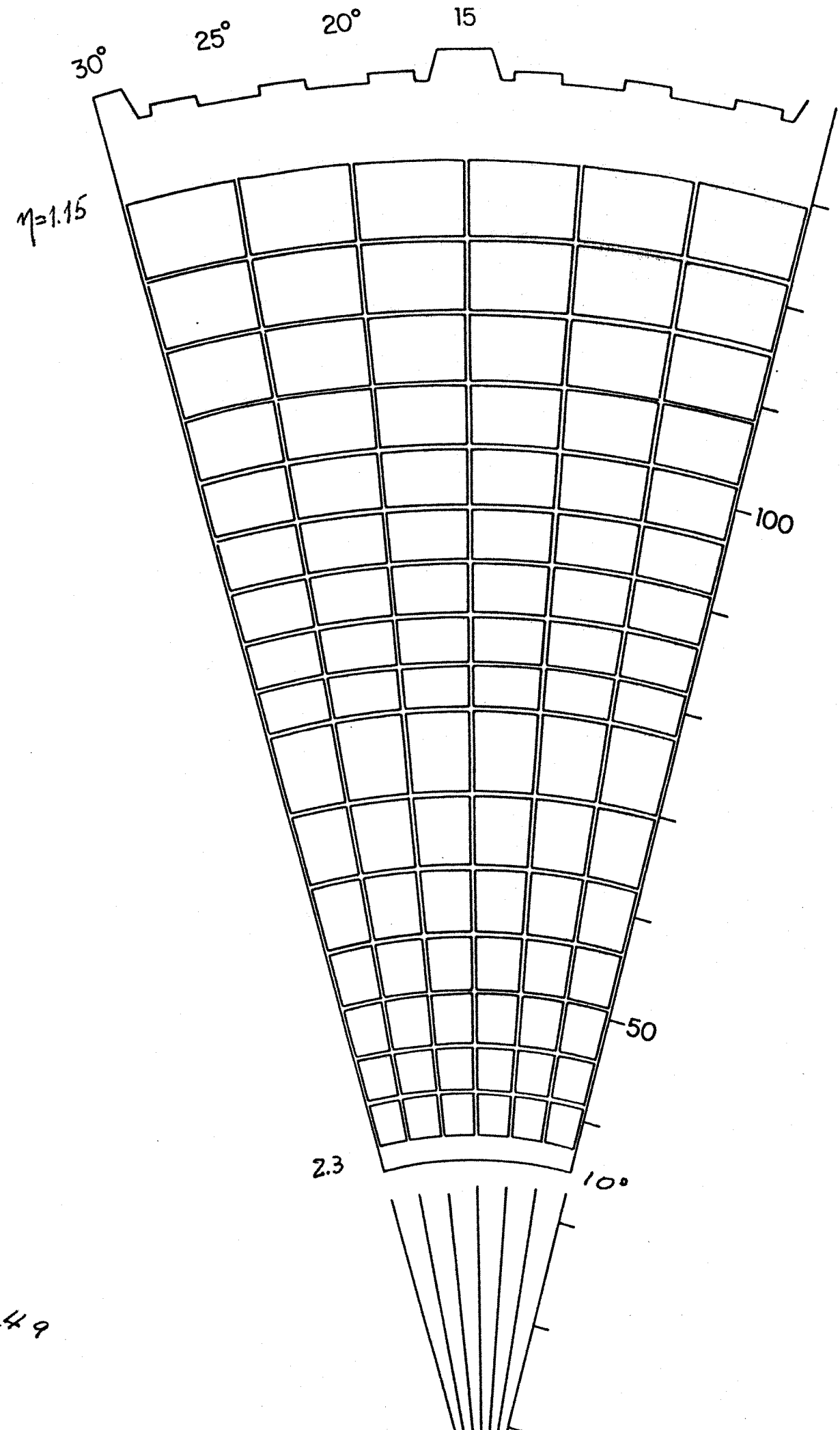

FIG. 4 9

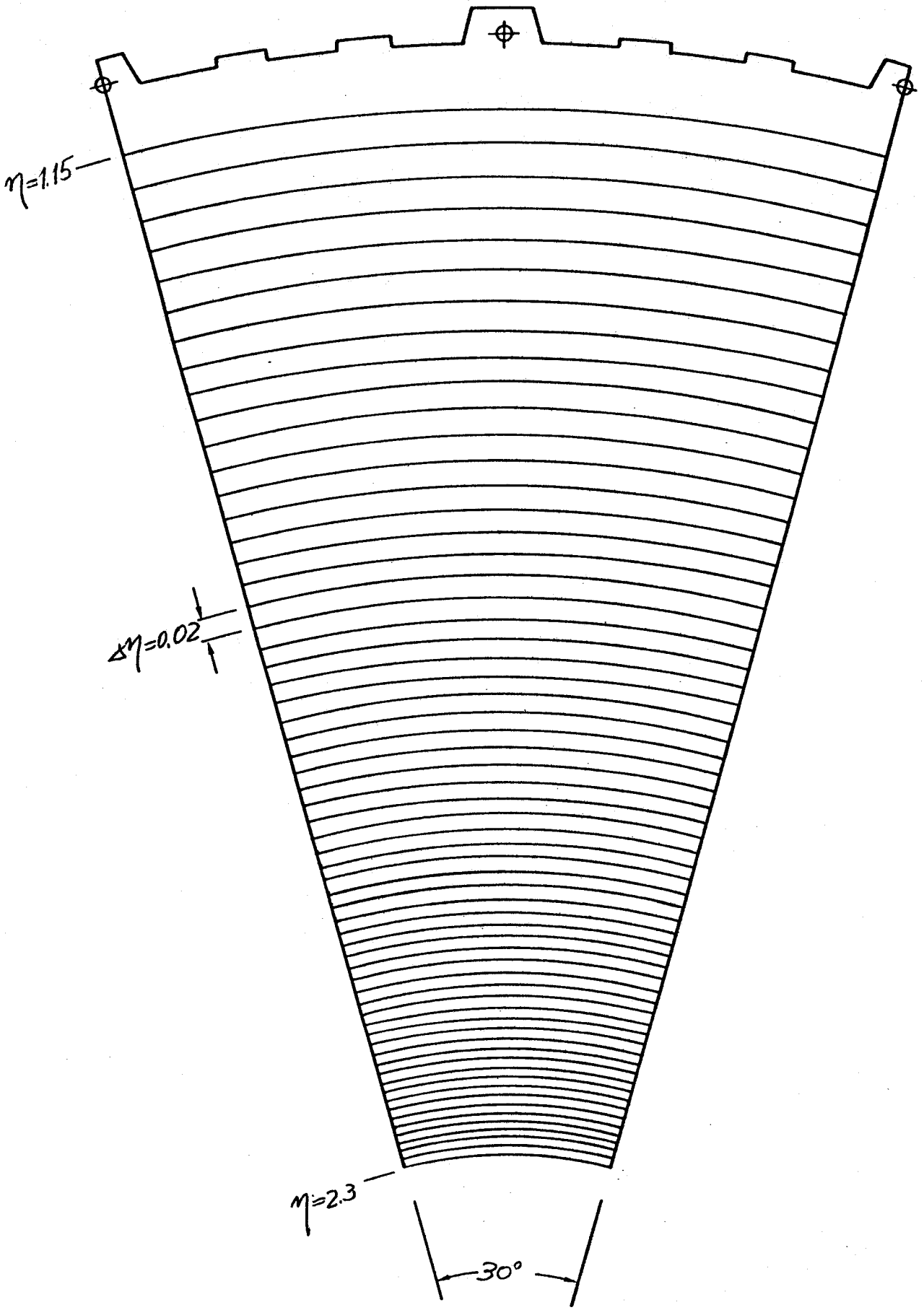

FIG. 46

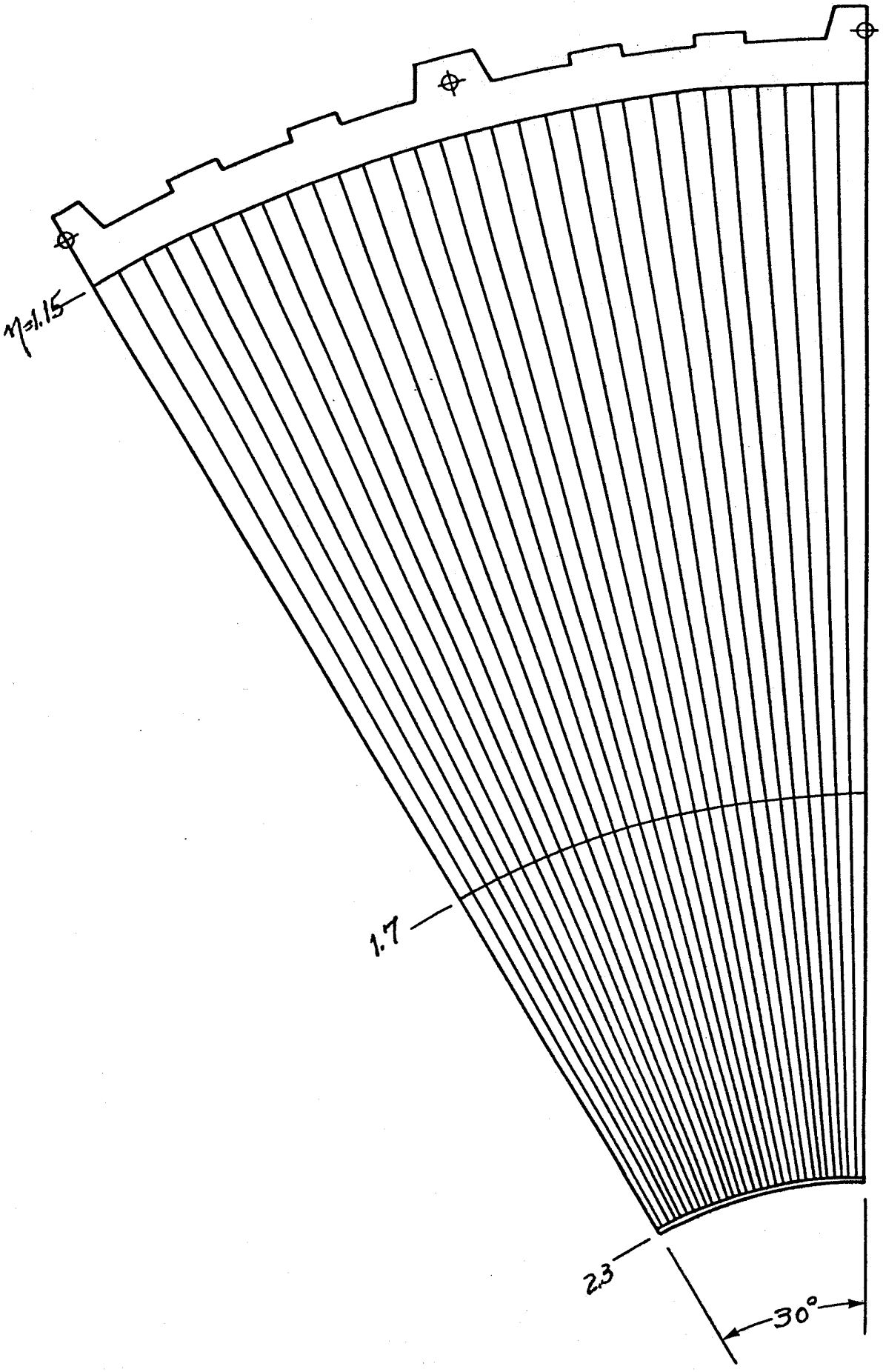

FIG. 4C

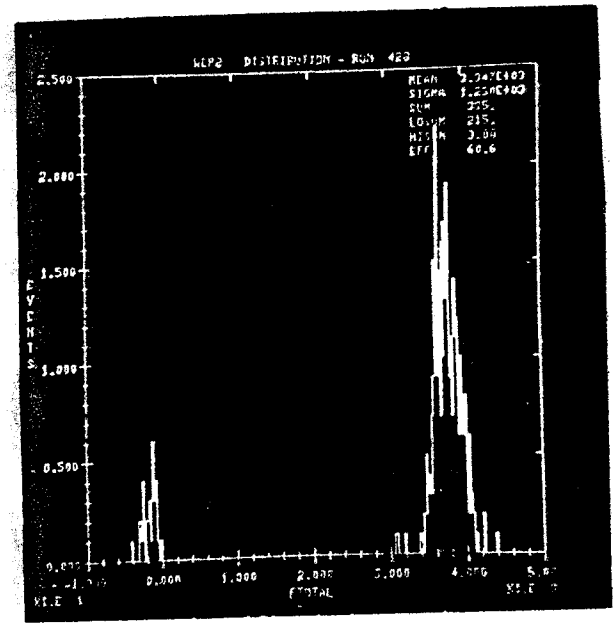

50 GeV
1.8 kV

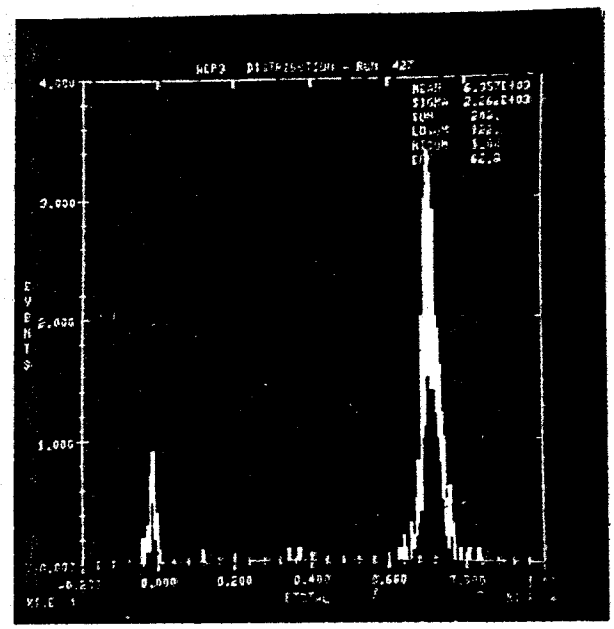

100 GeV
1.8 kV

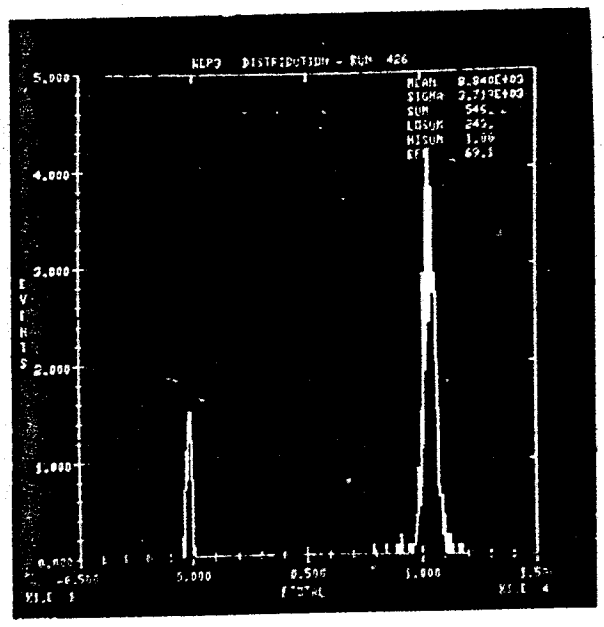

150 GeV
1.8 kV

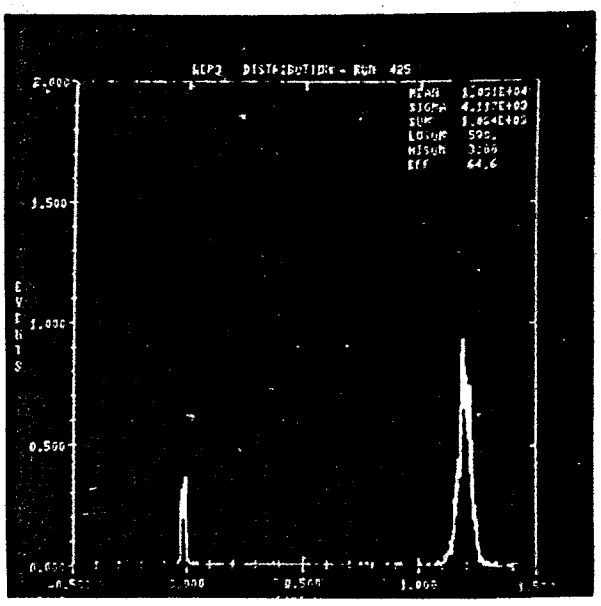

175 GeV
1.8 kV

Fig. 5

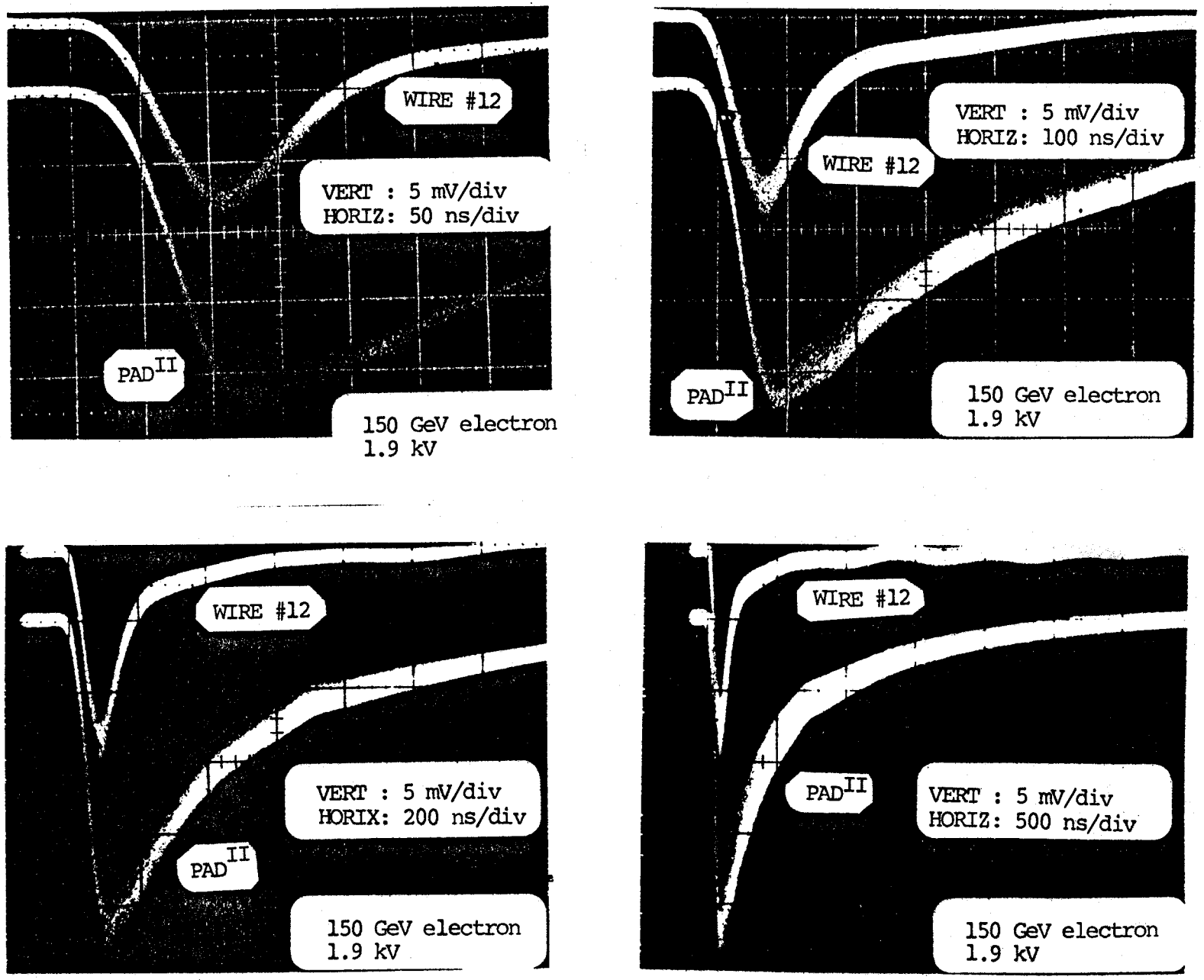
WIRE #12
VERT : 5 mV/div
HORIZ: 50 ns/div
PAD II
150 GeV electron
1.9 kV
WIRE #12
VERT : 5 mV/div
HORIZ: 100 ns/div
PAD II
150 GeV electron
1.9 kV
WIRE #12
VERT : 5 mV/div
HORIX: 200 ns/div
PAD II
150 GeV electron
1.9 kV
WIRE #12
PAD II
VERT : 5 mV/div
HORIZ: 500 ns/div
150 GeV electron
1.9 kV

FIG. 6

25, 50 GeV 75 GeV

PAD SIGNAL – TOTAL

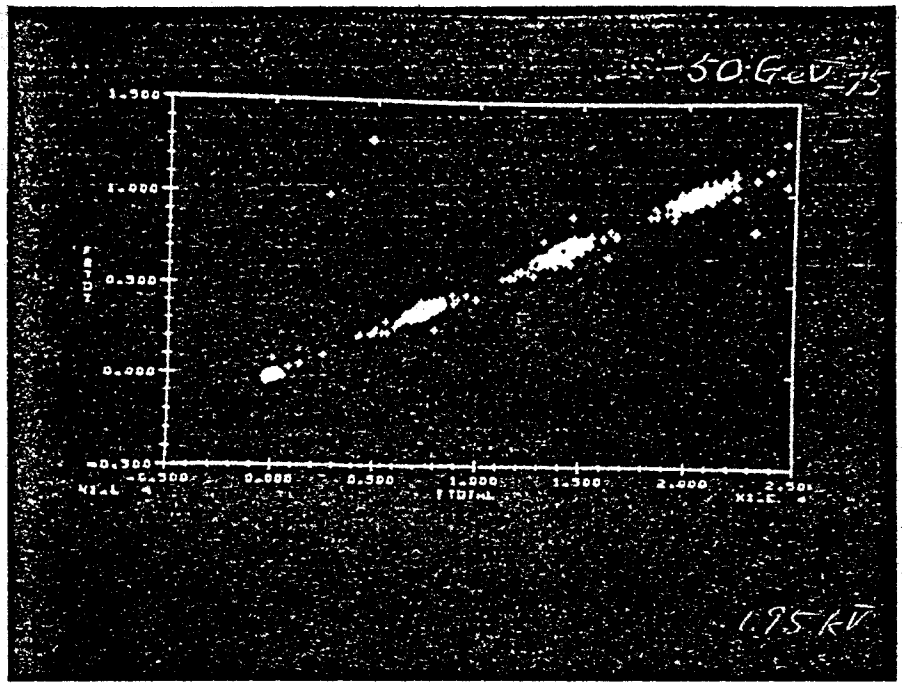

WIRE SIGNAL – TOTAL

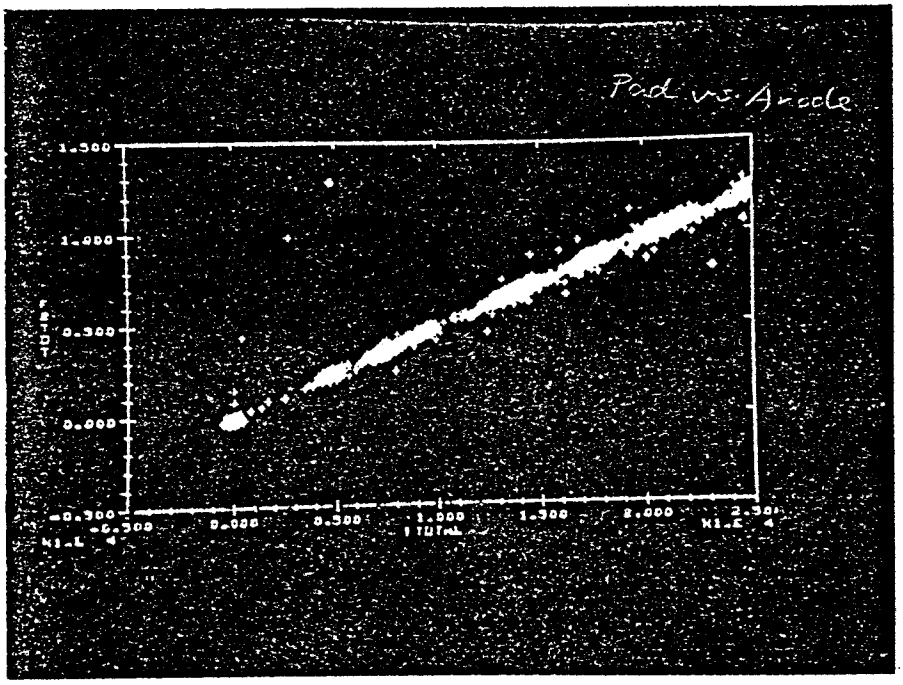

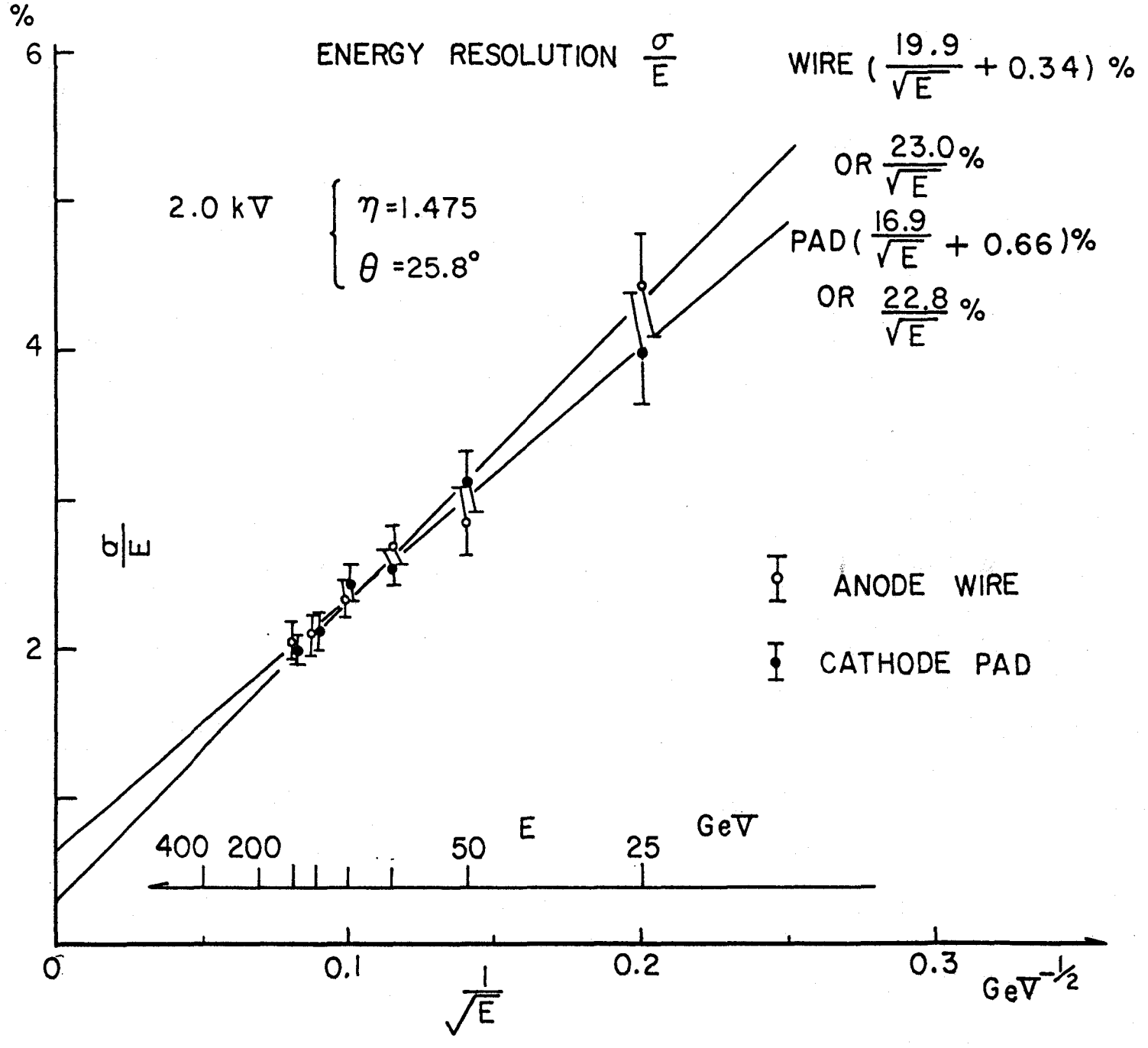
%
6
4
2
0
ENERGY RESOLUTION $\frac{\sigma}{E}$
WIRE $(\frac{19.9}{\sqrt{E}} + 0.34)$ %
OR $\frac{23.0}{\sqrt{E}}$ %
PAD $(\frac{16.9}{\sqrt{E}} + 0.66)$ %
OR $\frac{22.8}{\sqrt{E}}$ %
2.0 kV
η = 1.475
θ = 25.8°
σ/E
ANODE WIRE
CATHODE PAD
400 200 50 25
E GeV
0.1
0.2
0.3
$\frac{1}{\sqrt{E}}$
$GeV^{-1/2}$

Fig. 8

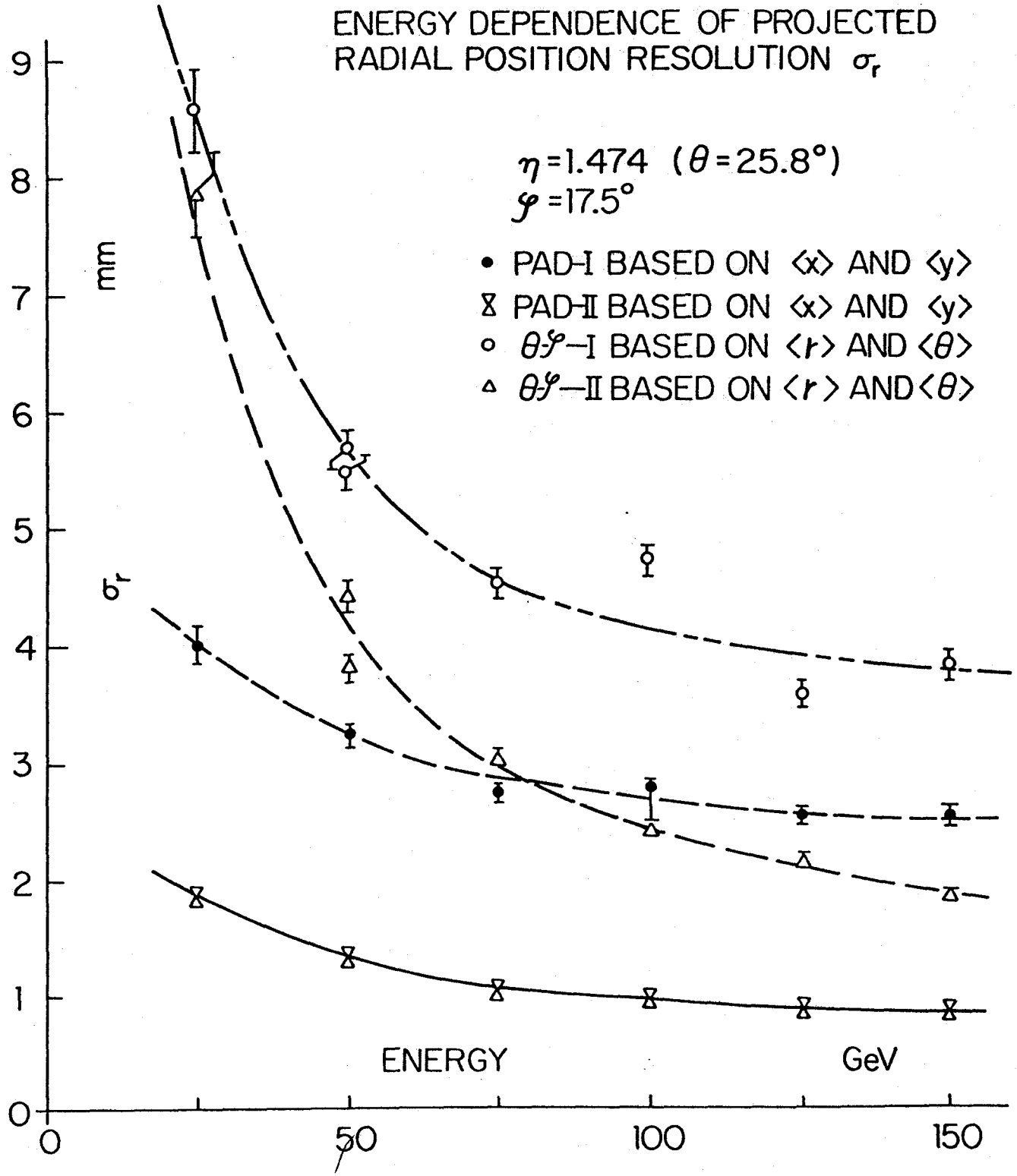
ENERGY DEPENDENCE OF PROJECTED
RADIAL POSITION RESOLUTION σ_r
$\eta = 1.474$ $(\theta = 25.8°)$
$\varphi = 17.5°$
• PAD-I BASED ON ⟨x⟩ AND ⟨y⟩
⧖ PAD-II BASED ON ⟨x⟩ AND ⟨y⟩
○ θφ—I BASED ON ⟨r⟩ AND ⟨θ⟩
△ θφ—II BASED ON ⟨r⟩ AND ⟨θ⟩
mm
σ_r
ENERGY
GeV
0
1
2
3
4
5
6
7
8
9
0
50
100
150

FIG. 9

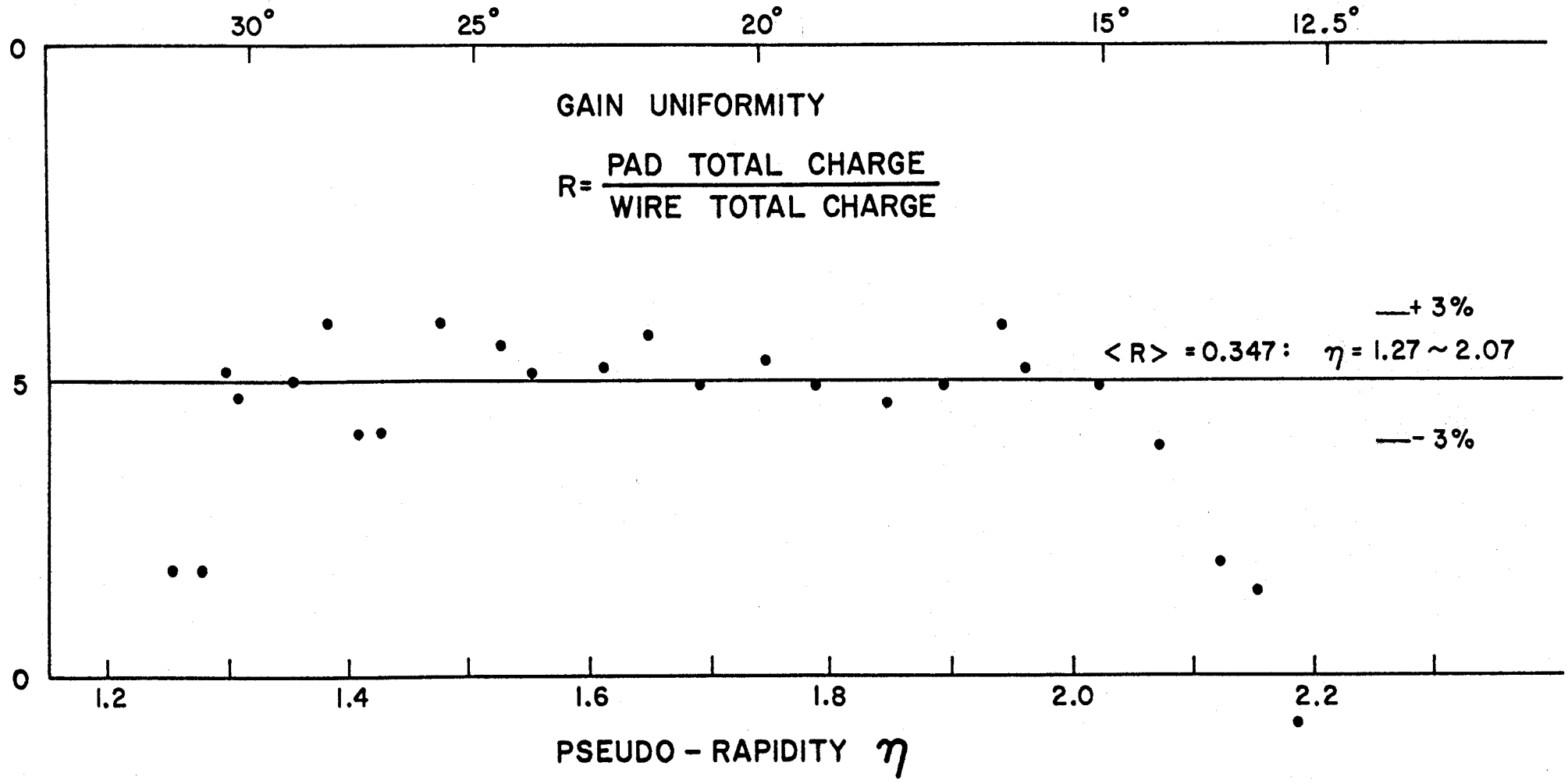
30°
25°
20°
15°
12.5°
0
GAIN UNIFORMITY
R= PAD TOTAL CHARGE / WIRE TOTAL CHARGE
+ 3%
<R> =0.347 : η = 1.27 ~ 2.07
5
- 3%
0
1.2
1.4
1.6
1.8
2.0
2.2
PSEUDO - RAPIDITY η

FIG. 10

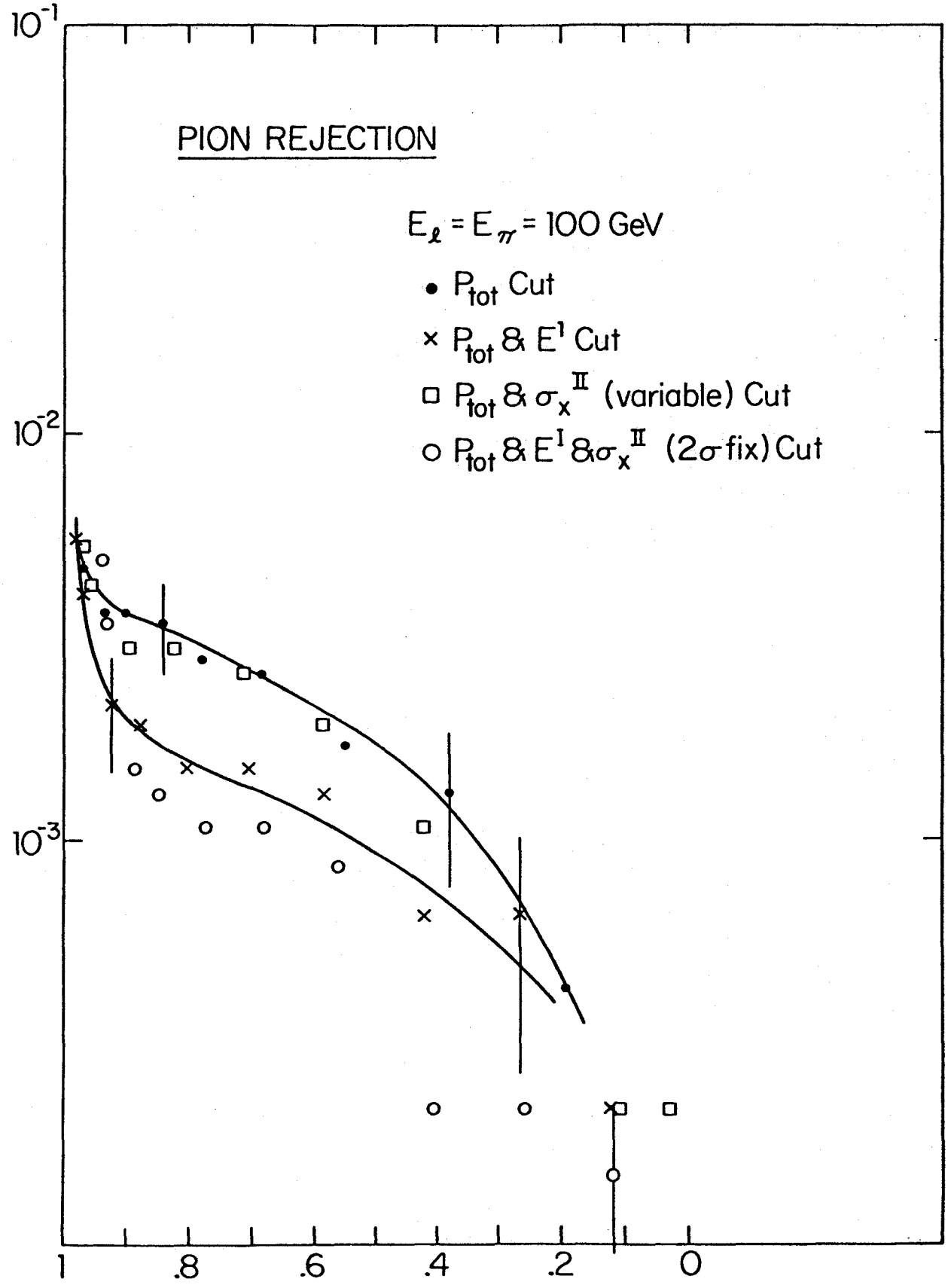
PION REJECTION
$E_\ell = E_\pi = 100$ GeV
• P_{tot} Cut
× P_{tot} & E^I Cut
□ P_{tot} & σ_x^{II} (variable) Cut
○ P_{tot} & E^I & σ_x^{II} (2σ fix) Cut
10^{-1}
10^{-2}
10^{-3}
1
.8
.6
.4
.2
0

FIG. 11 b.

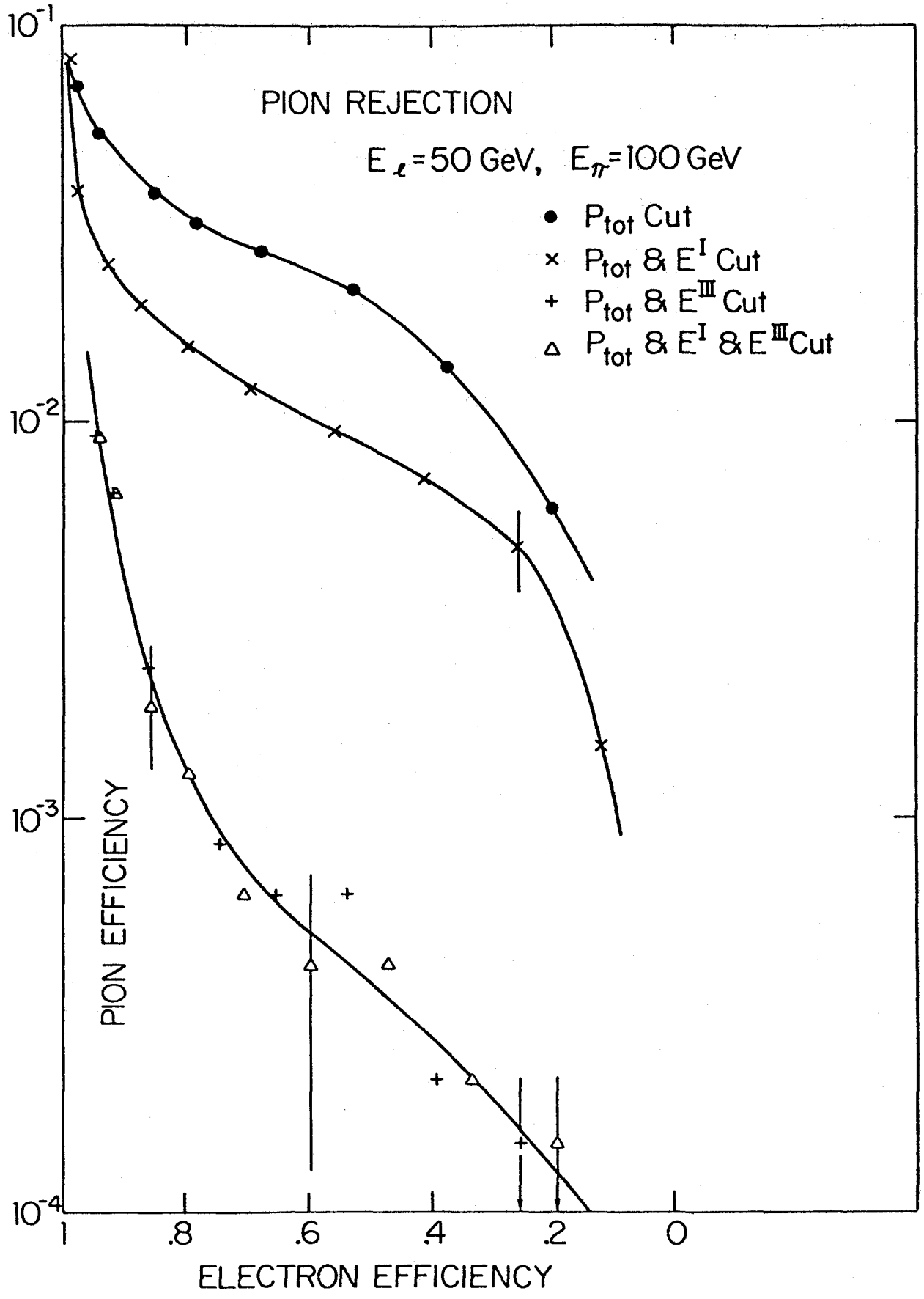
PION REJECTION
E_e = 50 GeV, E_π = 100 GeV
P_{tot} Cut
P_{tot} & E^I Cut
P_{tot} & E^{III} Cut
P_{tot} & E^I & E^{III} Cut
10^{-1}
10^{-2}
10^{-3}
10^{-4}
PION EFFICIENCY
1
.8
.6
.4
.2
0
ELECTRON EFFICIENCY

FIG 11a